PIV uncertainty propagation

Sciacchitano, Andrea; Wieneke, Bernhard

DOI
10.1088/0957-0233/27/8/084006

Publication date
2016

Document Version
Final published version

Published in
Measurement Science and Technology

PIV uncertainty propagation

2016 Meas. Sci. Technol. 27 084006

OPEN ACCESS
IOP Publishing
Made open access 26 August 2016
Measurement Science and Technology
Meas. Sci. Technol. **27** (2016) 084006 (16pp)
doi:10.1088/0957-0233/27/8/084006

PIV uncertainty propagation

Andrea Sciacchitano[1] **and Bernhard Wieneke**[2]

[1] Aerospace Engineering, TU Delft, Netherlands
[2] LaVision GmbH, Göttingen, Germany

E-mail: a.sciacchitano@tudelft.nl

Received 5 February 2016, revised 16 March 2016
Accepted for publication 30 March 2016
Published 29 June 2016

Abstract

This paper discusses the propagation of the instantaneous uncertainty of PIV measurements to statistical and instantaneous quantities of interest derived from the velocity field. The expression of the uncertainty of vorticity, velocity divergence, mean value and Reynolds stresses is derived. It is shown that the uncertainty of vorticity and velocity divergence requires the knowledge of the spatial correlation between the error of the x and y particle image displacement, which depends upon the measurement spatial resolution. The uncertainty of statistical quantities is often dominated by the random uncertainty due to the finite sample size and decreases with the square root of the effective number of independent samples. Monte Carlo simulations are conducted to assess the accuracy of the uncertainty propagation formulae. Furthermore, three experimental assessments are carried out. In the first experiment, a turntable is used to simulate a rigid rotation flow field. The estimated uncertainty of the vorticity is compared with the actual vorticity error root-mean-square, with differences between the two quantities within 5–10% for different interrogation window sizes and overlap factors. A turbulent jet flow is investigated in the second experimental assessment. The reference velocity, which is used to compute the reference value of the instantaneous flow properties of interest, is obtained with an auxiliary PIV system, which features a higher dynamic range than the measurement system. Finally, the uncertainty quantification of statistical quantities is assessed via PIV measurements in a cavity flow. The comparison between estimated uncertainty and actual error demonstrates the accuracy of the proposed uncertainty propagation methodology.

Keywords: particle image velocimetry, uncertainty quantification, uncertainty propagation, linear error propagation, spatial resolution

(Some figures may appear in colour only in the online journal)

List of symbols

d	spacing between adjacent grid points
f	focal length of a lens
F	general function
FOV	field of view
$f\#$	f-number of a lens
f_{acq}	acquisition frequency
L_{sr}	spatial resolution length
L^*_{sr}	spatial resolution length relative to the vector spacing d
N	number of measured variables; number of acquired samples
N_{eff}	effective number of independent samples
n_{pix}	linear size (in pixels) of the PIV interrogation window
R_{uu}, R_{vv}, R_{ww}	Reynolds normal stresses
$R_{uu,\,true}$, $R_{uu,\,corr}$	true/corrected Reynolds normal stress
R_{uv}	Reynolds shear stress
T	total recording time
TI	turbulence intensity
T_{int}	integral time scale
TKE	turbulent kinetic energy
u	horizontal velocity component
$\overline{u}$	mean velocity
u'	fluctuating velocity
u'_{true}	true fluctuating velocity (in absence of measurement errors)

U_x	uncertainty of the quantity x
$\overline{U_u^2}$	mean-square of the uncertainty of u
$U_{\overline{U_u^2}}$	uncertainty of the mean-square of the uncertainty of u
U_u^{rms}	root-mean-square averaged uncertainty of u
v	vertical velocity component
w	spanwise velocity component
x	measured variable; horizontal coordinate
$\overline{x}$	mean value of the quantity x
y	derived quantity of interest; vertical coordinate
Δt	time interval between successive samples (inverse of the acquisition frequency)
δx	measurement error of the quantity x
$\rho(x,y)$, ρ_{xy}	cross-correlation coefficient between x and y
$\rho(a)$	cross-correlation coefficient between two samples at temporal or spatial separation a
σ_x	standard deviation of x
σ_{U_u}	standard deviation of the uncertainty of u
$\sigma^2_{u,\mathrm{err}}$	variance of u due to measurement errors
$\sigma^2_{u,\mathrm{fluct}}$	variance of u due to physical flow fluctuations
σ^2_{xy}	covariance between x and y
σ^2_x	variance of x
ω	vorticity
ω_0	reference vorticity
ω_z	out-of-plane vorticity component

1. Introduction

Uncertainty quantification in particle image velocimetry (PIV) is crucial to determine an interval that contains the measurement error. Several a-posteriori PIV uncertainty quantification methods have been recently proposed to estimate the unknown error for every velocity vector in the flow field.

In the '*uncertainty surface*' method by Timmins *et al* (2012), the recorded images are analyzed to quantify the magnitude of relevant error sources (particle image size, particle density, displacements and shear). Comparing to previously computed errors using synthetic data leads to uncertainty estimation for every vector. The '*peak ratio*' method by Charonko and Vlachos (2013) makes use of an empirical relation between uncertainty and the ratio between the highest and the second highest correlation peak. Further advances on the quantification of the measurement uncertainty based on the cross-correlation signal-to-noise ratio have been proposed by Xue *et al* (2014). In the '*image matching*' or '*particle disparity*' method by Sciacchitano *et al* (2013), the measured displacement field is used to deform the recorded images, and the residual disparity in the position of matching particle images leads to an estimate of the uncertainty of the displacement vector. Finally, the '*correlation statistics*' method by Wieneke (2015) analyzes the contribution of all pixel intensities to a possible asymmetry of the correlation peak, which is related to the uncertainty of the displacement vector. All these methods allow the a-posteriori quantification of the instantaneous measurement uncertainty. A thorough comparison of their performances in different imaging and flow conditions is reported in Sciacchitano *et al* (2015), where the dedicated experimental data from Neal *et al* (2015) is used.

In many applications, PIV measurements are conducted to investigate flow properties derived from the velocity field, which can be instantaneous (e.g. vorticity, velocity divergence, acceleration, turbulence dissipation rate, pressure) or statistical quantities (e.g. time average and Reynolds stresses). Therefore, once the uncertainties of the instantaneous velocity components are estimated, they need to be propagated into the derived quantities of interest. The quantification of the uncertainty of derived quantities relies upon the following considerations:

i. the uncertainty of the velocity components propagates to that of the derived quantity of interest;
ii. the correlation (in space, time and/or inter-component) of velocity components affects the uncertainty of derived quantities;
iii. for statistical quantities, additional uncertainty is due to the finite number of samples N, which yields lack of statistical convergence.

The works of Wilson and Smith (2013a, 2013b) provide upper and lower uncertainty bounds for a number of statistical quantities, such as average, variance and covariance. In their analysis, the authors considered the contributions of random errors, mainly due to the finite sample size, and unknown time-dependent systematic errors. For velocity variance and covariance, the lower uncertainty bound was found to be larger than the upper uncertainty bound because spurious fluctuations tend to elevate the time-averaged measured fluctuations, yielding an error in the negative direction. In the work presented here, uncertainty quantification is provided for many commonly used derived quantities in PIV processing, both statistical and instantaneous. Following Coleman and Steele (2009), we assume that each systematic error whose sign and magnitude are known has been removed by correction. Thus the paper focuses on random errors and uncertainties. The work discusses the basic concepts of uncertainty propagation and its applications for flow properties of interest in typical PIV measurements, such as vorticity, mean velocity and Reynolds stresses. Furthermore, a correction of the Reynolds stresses based on the magnitude of the noisy fluctuations is proposed.

2. Uncertainty propagation methodology

2.1. Basic concepts

Let us consider a derived quantity of interest y, which is a general function F of N measured variables x_i, with $i = 1, 2, \ldots, N$.

$$y = F(x_1, x_2, \ldots, x_N) \tag{1}$$

Assuming that each variable x_i has a standard deviation σ_{x_i}, and given sufficient linearity of F, the variance of y can be approximated by the variance-covariance matrix of F (Bendat and Piersol 2010):

$$\mathrm{var}(y) = \sum_{i=1}^{N}\sum_{j=1}^{N}\frac{\partial F}{\partial x_i}\frac{\partial F}{\partial x_j}\,\mathrm{cov}(x_i,x_j)$$
$$= \sum_{i=1}^{N}\left(\frac{\partial F}{\partial x_i}\right)^2 \mathrm{var}(x_i) + 2\sum_{i=1}^{N-1}\sum_{j=i+1}^{N}\frac{\partial F}{\partial x_i}\frac{\partial F}{\partial x_j}\,\mathrm{cov}(x_i,x_j) \quad (2)$$

or in another notation:

$$\sigma_y^2 = \sum_{i=1}^{N}\sum_{j=1}^{N}\frac{\partial F}{\partial x_i}\frac{\partial F}{\partial x_j}\rho(x_i,x_j)\,\sigma_{x_i}\sigma_{x_j}$$
$$= \sum_{i=1}^{N}\left(\frac{\partial F}{\partial x_i}\right)^2\sigma_{x_i}^2 + 2\sum_{i=1}^{N-1}\sum_{j=i+1}^{N}\frac{\partial F}{\partial x_i}\frac{\partial F}{\partial x_j}\rho(x_i,x_j)\,\sigma_{x_i}\sigma_{x_j} \quad (3)$$

where $\rho(x_i, x_j)$ is the cross-correlation coefficient between x_i and x_j, defined by:

$$\rho(x_i,x_j) = \mathrm{cov}(x_i,x_j)\ /\ \sigma_{x_i}\sigma_{x_j} \quad (4)$$

Notice that when x_i and x_j are independent, then $\rho(x_i, x_j) = 0$ and equation (3) reduces to:

$$\sigma_y^2 = \sum_{i=1}^{N}\left(\frac{\partial F}{\partial x_i}\right)^2\sigma_{x_i}^2 \quad (5)$$

Equation (3) can be interpreted in two ways. First, assuming that the set of input variables x_i is measured many times, each time yielding an output variable y_j, the standard deviation σ_y provides a measure of the fluctuation of the derived y_j's. Secondly, σ_y provides a measure of the uncertainty U_y of y for a single measurement given the standard uncertainties U_{x_i} of each input variable x_i (Coleman and Steele 2009):

$$U_y^2 = \sum_{i=1}^{N}\left(\frac{\partial F}{\partial x_i}\right)^2 U_{x_i}^2 + 2\sum_{i=1}^{N-1}\sum_{j=i+1}^{N}\frac{\partial F}{\partial x_i}\frac{\partial F}{\partial x_j}\rho(\delta x_i,\delta x_j)\,U_{x_i}U_{x_j} \quad (6)$$

where $\rho(\delta x_i, \delta x_j)$ is now the cross-correlation coefficient between the *errors* of x_i and x_j, which are indicated with δx_i and δx_j, respectively. This equation will be used extensively in the following.

In the present work, the uncertainty of instantaneous velocity components is quantified with the correlation statistics method (Wieneke 2015). Equation (6) shows that the evaluation of the uncertainty of y requires the knowledge of the cross-correlation between velocity vectors separated in time or space or inter-component. Most PIV-UQ methods are unable to compute such values from single interrogation windows. The values of ρ are usually determined beforehand for a particular set of PIV processing parameter e.g. by Monte-Carlo simulation with synthetic data, similar to the uncertainty surface method by Timmins *et al* (2012), which analyses the local imaging and flow conditions and looks up the corresponding potentially skewed and biased error distribution. Further details on the computation of the error spatial/temporal correlation are given in next sections.

2.2. Time-averaged statistical quantities

Given a set of samples $x = \{x_1, x_2, \ldots, x_N\}$ recorded over time, the temporal mean value, standard deviation and variance of x are defined as, respectively:

$$\overline{x} = \frac{1}{N}\sum_{i=1}^{N}x_i \quad (7)$$

$$\sigma_x = \sqrt{\frac{1}{N-1}\sum_{i=1}^{N}(x_i-\overline{x})^2} \quad (8)$$

$$\sigma_x^2 = \frac{1}{N-1}\sum_{i=1}^{N}(x_i-\overline{x})^2 \quad (9)$$

Given two sets of samples x and y, the covariance $\mathrm{cov}(x, y)$ or σ_{xy}^2 between them is defined as:

$$\sigma_{xy}^2 = \frac{1}{N-1}\sum_{i=1}^{N}(x_i-\overline{x})(y_i-\overline{y}) \quad (10)$$

Notice that equations (7)–(10) provide the mean, standard deviation and variance for the *sample population*. These values are estimates of the corresponding values for the *parent population*, which comprises the totality of all samples (not only those acquired during the measurement). The accuracy of the estimate increases for increasing N; the estimates are exact for $N \to \infty$.

Assuming that the samples are independent and follow a normal distribution of standard deviation σ_x, the standard uncertainty of the above quantities is (Benedict and Gould 1996):

Uncertainty of mean:

$$U_{\overline{x}} = \frac{\sigma_x}{\sqrt{N}} \quad (11)$$

Uncertainty of standard deviation:

$$U_{\sigma_x} = \frac{\sigma_x}{\sqrt{2(N-1)}} \quad (12)$$

Uncertainty of variance:

$$U_{\sigma_x^2} = \sigma_x^2\sqrt{\frac{2}{N-1}} \quad (13)$$

Finally, the uncertainty of the covariance is (Bendat and Piersol 2010):

$$U_{\sigma_{xy}^2} = \sigma_x\sigma_y\sqrt{\frac{1+\rho_{xy}^2}{N-1}} \quad (14)$$

where ρ_{xy} is the cross-correlation coefficient between x and y.

These equations are valid for sufficiently large N. Ahn and Fessler (2003) report that for $N \geqslant 30$ these formulae are accurate within 1%. For a smaller number of samples, the formulae typically underestimate the actual standard uncertainty by up to 10%, and correction factors should be used for the mean, standard deviation and variance to make them unbiased (Coleman and Steele 2009). The results of equations (11)–(14) will be used in the following for determining the uncertainty of statistical quantities of interest in turbulent flows.

2.2.1. Uncertainty of the mean velocity. Consider the generic velocity component u. Based on equations (7) and (11), the uncertainty of the mean velocity $\overline{u}$ is:

$$U_{\overline{u}} = \frac{\sigma_u}{\sqrt{N}} \tag{15}$$

Analogous equations are obtained for the v and w velocity components. In equation (15), systematic uncertainties due to spatial modulation errors or peak locking are not taken into account. The standard deviation σ_u contains both the true velocity fluctuations ($\sigma_{u,\ \mathrm{fluct}}$) and the measurement errors ($\sigma_{u,\mathrm{err}}$):

$$\sigma_u^2 = \sigma_{u,\ \mathrm{fluct}}^2 + \sigma_{u,\ \mathrm{err}}^2 \approx \sigma_{u,\ \mathrm{fluct}}^2 + \overline{U_u^2} \tag{16}$$

where U_u is the uncertainty of the instantaneous velocity component and $\overline{U_u^2}$ is the mean-square of U_u. The right-hand-side of equation (16) is obtained by considering that the error variance $\sigma_{u,\ \mathrm{err}}^2$ is approximately equal to the uncertainty mean-square $\overline{U_u^2}$ for accurate uncertainty quantification methods (see appendix of Sciacchitano *et al* 2015).

When the samples are not independent, the parameter N of equation (15) must be substituted with the effective number of independent samples N_{eff}, as discussed in section 2.2.3.

2.2.2. Uncertainty of Reynolds stress. The Reynolds stress plays a crucial role in turbulent flows because it represents the rate of mean momentum transfer by turbulent fluctuations. In this section, the expression of the uncertainty is derived for the Reynolds normal stress and for the Reynolds shear stress.

Reynolds normal stress. The Reynolds normal stress for the x-velocity component u is defined as the variance of u:

$$R_{uu} = \overline{u'^2} = \sigma_u^2 = \frac{1}{N-1}\sum_{i=1}^{N}(u_i - \overline{u})^2 \tag{17}$$

where u' is the fluctuating part of u: $u' = u - \overline{u}$. Due to its definition, the uncertainty of R_{uu} is computed with equation (13):

$$U_{R_{uu}} = \sigma_u^2\sqrt{\frac{2}{N-1}} \cong \sigma_u^2\sqrt{\frac{2}{N}} = R_{uu}\sqrt{\frac{2}{N}} \tag{18}$$

It is assumed that the samples are statistically independent. If not, N must again be substituted with the effective number of independent samples N_{eff} (section 2.2.3). As discussed in section 2.2.1, σ_u contains both the effects of true velocity fluctuations and spurious fluctuations due to noise. The latter yield an over-estimate for R_{uu} with respect to the true value $R_{uu,\ \mathrm{true}}$:

$$R_{uu} = R_{uu,\mathrm{true}} + \sigma_{u,\mathrm{err}}^2 = R_{uu,\mathrm{true}} + \overline{U_u^2} \tag{19}$$

When the uncertainty of the measured velocity is known, a corrected (more accurate) estimate of R_{uu} can be retrieved by subtracting the spurious fluctuations mean square $\overline{U_u^2}$from the measured Reynolds stress:

$$R_{uu,\mathrm{corr}} = R_{uu} - \overline{U_u^2} \tag{20}$$

Thus, according to equation (6), the uncertainty of the corrected normal Reynolds stress estimate $R_{uu,\ \mathrm{corr}}$, indicated with $U_{R_{uu,\mathrm{corr}}}$, is given by:

$$U_{R_{uu,\mathrm{corr}}} = \sqrt{U_{R_{uu}}^2 + U_{\overline{U_u^2}}^2} \tag{21}$$

The latter is composed by two components: (a) the uncertainty of the measured Reynolds stress, which is given by equation (18); (b) the uncertainty of the spurious fluctuations mean square $\overline{U_u^2}$. Notice that U_u^2 can only assume positive values, therefore its distribution is better approximated by a log-normal distribution rather than by a Gaussian distribution. At least when approximating the distribution with a Gaussian distribution with positive mean, an analytical expression of the uncertainty of $\overline{U_u^2}$ can be derived using equation (6):

$$U_{\overline{U_u^2}} = \frac{2}{\sqrt{N}}\,\sigma_{U_u}\overline{U_u}\cdot\sqrt{1 + \frac{\sigma_{U_u}^2}{2\overline{U_u}^2}} \tag{22}$$

The accuracy of equation (22) is assessed in section 3.1. Combining both equations (18) and (22), the uncertainty of $R_{uu,\ \mathrm{corr}}$ is:

$$U_{R_{uu,\mathrm{corr}}} = \sqrt{R_{uu}^2 + \left(\sqrt{2}\,\sigma_{U_u}\overline{U_u}\cdot\sqrt{1 + \frac{\sigma_{U_u}^2}{2\overline{U_u}^2}}\right)^2}\cdot\sqrt{\frac{2}{N}} \tag{23}$$

In many applications, the measurement error is small with respect to the actual velocity fluctuations, therefore the term within brackets is negligible and equation (23) reduces to:

$$U_{R_{uu,\mathrm{corr}}} = R_{uu}\cdot\sqrt{\frac{2}{N}} \tag{24}$$

In practice, the uncertainty of the Reynolds normal stress according to (23) and (24) is often strongly underestimated for two reasons. First, the subtraction of equation (20) is subject to the accuracy of the uncertainty quantification method itself. As shown by Sciacchitano *et al* (2015), the uncertainty estimations of state-of-the-art UQ methods may deviate from the true errors by as much as a factor two for different flow and imaging conditions. Secondly, the finite spatial resolution of the PIV processing algorithm does not allow resolving fluctuations of length scale smaller than about the interrogation window. This may lead to a substantial underestimation of R_{uu} depending on Reynolds number, turbulent level and imaging magnification.

It is important to remark here that the computation of the uncertainty of R_{uu} according to equation (18) does not require the knowledge of the uncertainty of the instantaneous velocity. On the other hand, in order to compute the corrected value $R_{uu,\ \mathrm{corr}}$, the uncertainty of the instantaneous velocity must be known.

Turbulent kinetic energy. The turbulent kinetic energy TKE is defined as half of the sum of the Reynolds normal stresses:

$$\mathrm{TKE} = \frac{1}{2}\overline{u_i'u_i'} = \frac{1}{2}(R_{uu} + R_{vv} + R_{ww}) \tag{25}$$

Based on the error propagation formula (6), the uncertainty of the TKE is equal to:

$$U_{\mathrm{TKE}} = \frac{1}{2}\sqrt{U_{R_{uu}}^2 + U_{R_{vv}}^2 + U_{R_{ww}}^2} \tag{26}$$

Assuming $N \gg 1$ and that the instantaneous measurement uncertainty is negligible with respect to the velocity fluctuations, the result of equation (24) can be used and the expression of U_{TKE} reduces to:

$$U_{\mathrm{TKE}} = \sqrt{R_{uu}^2 + R_{vv}^2 + R_{ww}^2} \cdot \sqrt{\frac{1}{2N}} \tag{27}$$

When R_{ww} is unknown (e.g. in planar PIV, which only provides two velocity components), its value can be estimated as $R_{ww} = (R_{uu} + R_{vv})/2$ under the assumption of isotropic turbulence.

Reynolds shear stress. The Reynolds shear stress R_{uv} is defined as the covariance of the u and v velocity components:

$$\begin{aligned} R_{uv} &= \overline{u'v'} = \frac{1}{N-1}\sum_{i=1}^{N} u_i' v_i' = \frac{1}{N-1}\sum_{i=1}^{N}(u_i - \overline{u})(v_i - \overline{v}) \\ &= \rho_{uv}\sigma_u\sigma_v \end{aligned} \tag{28}$$

The quantity ρ_{uv} is the cross-correlation coefficient between the velocity components u and v. Assuming that the velocity fluctuations are affected by error δu and δv, respectively, and that the error of the time-averaged velocity is negligible, equation (28) becomes:

$$\begin{aligned} R_{uv} &= \frac{1}{N-1}\sum_{i=1}^{N}(u_{i,\mathrm{true}}' + \delta u)(v_{i,\mathrm{true}}' + \delta v) \\ &= \frac{1}{N-1}\sum_{i=1}^{N}(u_{i,\mathrm{true}}' v_{i,\mathrm{true}}' + u_{i,\mathrm{true}}'\delta v + v_{i,\mathrm{true}}'\delta u + \delta u\delta v) \\ &= \frac{1}{N-1}\sum_{i=1}^{N}(u_{i,\mathrm{true}}' v_{i,\mathrm{true}}' + \delta u\delta v) \\ &= R_{uv,\mathrm{true}} + \rho_{\delta u\delta v}\sigma_{\delta u}\sigma_{\delta v} \cong R_{uv,\mathrm{true}} + \rho_{\delta u\delta v}\sqrt{\overline{U_u^2}\,\overline{U_v^2}} \end{aligned} \tag{29}$$

In equation (29), $\rho_{\delta u\delta v}$ is the cross-correlation coefficient between the errors of the two velocity components. The true velocity fluctuations are assumed to be independent of the measurement errors, thus cancelling the cross-terms $\sum_{i=1}^{N}(u_{i,\mathrm{true}}'\delta v)$ and $\sum_{i=1}^{N}(v_{i,\mathrm{true}}'\delta u)$. As a consequence, the Reynolds shear stress R_{uv} exhibits a systematic error (equal to $\rho_{\delta u\delta v}\sqrt{\overline{U_u^2}\,\overline{U_v^2}}$) only if δu and δv are correlated ($\rho_{\delta u\delta v} \neq 0$); however, this is typically not the case for planar 2 C-PIV. Conversely, for stereo-PIV there may be non-zero inter-component correlations dependent on the experimental setup of the two cameras relative to the x- and y-axis. The uncertainty of R_{uv} is obtained by applying the covariance uncertainty equation (14):

$$U_{R_{uv}} = \sigma_u\sigma_v \cdot \sqrt{\frac{1+\rho_{uv}^2}{N-1}} \tag{30}$$

The uncertainty of the Reynolds shear stress has a minimum value of $\sigma_u\sigma_v/\sqrt{N-1}$ when u and v are uncorrelated and increases with higher correlation between the two velocity components.

2.2.3. Effective number of independent samples. Consider a generic statistical quantity, as the mean $\overline{x}$. In this section we will show that if the N samples from which $\overline{x}$ is computed are not independent, a larger uncertainty of $\overline{x}$ is expected. In fact, from equation (6) it is obtained:

$$U_{\overline{x}}^2 = \sum_{i=1}^{N}\sum_{j=1}^{N}\frac{1}{N^2}\rho(x_i, x_j)\sigma_x^2 \tag{31}$$

having assumed a constant underlying fluctuation distribution $\sigma_{x_i} = \sigma_{x_j} = \sigma_x$. The auto-correlation coefficient $\rho(x_i, x_j)$ can be written as:

$$\rho(x_i, x_j) = \rho(x_i, x_{i+n}) = \rho(n\Delta t) \tag{32}$$

with Δt the inverse of the sampling frequency. The auto-correlation coefficient ρ is a function of the time separation $n\Delta t$ between samples x_i and $x_j = x_{i+n}$. As a result, equation (31) can be written as:

$$U_{\overline{x}}^2 = \frac{\sigma_x^2}{N^2}\sum_{i=1}^{N}\sum_{n=1-i}^{N-i}\rho(x_i, x_{i+n}) = \frac{\sigma_x^2}{N^2}\sum_{i=1}^{N}\sum_{n=1-i}^{N-i}\rho(n\Delta t) \tag{33}$$

The quantity $\rho(n\Delta t)$ is equal to one for $n = 0$ and decays to zero for increasing n. Furthermore, $\rho(n\Delta t)$ is an even function: $\rho(n\Delta t) = \rho(-n\Delta t)$. Assuming $N \to \infty$ and neglecting the edge effects in the summation, equation (33) becomes:

$$\begin{aligned} U_{\overline{x}}^2 &= \frac{\sigma_x^2}{N^2}\sum_{i=1}^{N}\sum_{n=-\infty}^{+\infty}\rho(n\Delta t) = \frac{\sigma_x^2}{N^2}N\sum_{n=-\infty}^{+\infty}\rho(n\Delta t) \\ &= \sigma_x^2\frac{\sum_{n=-\infty}^{+\infty}\rho(n\Delta t)}{N} \end{aligned} \tag{34}$$

Defining the effective number of independent samples as:

$$N_{\mathrm{eff}} = \frac{N}{\sum_{n=-\infty}^{+\infty}\rho(n\Delta t)} \tag{35}$$

leads to:

$$U_{\overline{x}}^2 = \frac{\sigma_x^2}{N_{\mathrm{eff}}} \text{ or } U_{\overline{x}} = \frac{\sigma_x}{\sqrt{N_{\mathrm{eff}}}} \tag{36}$$

Typically, the summation of equation (35) is stopped when the correlation value reaches zero for the first time. Notice that when the samples are uncorrelated, then $\rho(n\Delta t)$ is 1 for $n = 0$ and zero otherwise, so in this case $N_{\mathrm{eff}} = N$. Conversely, when the samples are correlated then $\sum_{n=-\infty}^{+\infty}\rho(n\Delta t) > 1$; therefore N_{eff} is smaller than N, thus the uncertainty of the mean value is larger.

The integral time scale T_{int} is defined as the integral of the auto-correlation function $\rho(t)$ of the time series $x(t)$ (George *et al* 1978):

$$T_{\mathrm{int}} = \int_0^{\infty}\rho(t)\mathrm{d}t \tag{37}$$

T_{int} is a measure of the time interval over which $x(t)$ is dependent on itself. For time intervals large compared to T_{int}, $x(t)$ becomes statistically independent of itself. Then, the effective number of independent samples can be written as a function of the observation time T and the integral time scale T_{int}:

$$N_{\text{eff}} = \frac{N}{\sum_{n=-\infty}^{+\infty} \rho(n\Delta t)} = \frac{N \cdot \Delta t}{\sum_{n=-\infty}^{+\infty} \rho(n\Delta t) \cdot \Delta t} \approx \frac{T}{\int_{-\infty}^{+\infty} \rho(\mathrm{d}t)\mathrm{d}t} = \frac{T}{2\int_{0}^{+\infty} \rho(\mathrm{d}t)\mathrm{d}t} = \frac{T}{2T_{\text{int}}} \quad (38)$$

The relevance of equations (36) and (38) for experimental measurements in turbulent flows is discussed by Tennekes and Lumley (1972) among others. The equations illustrate the fact that, when $\Delta t < T_{\text{int}}$ and the total observation time T is fixed, increasing the sampling frequency and therefore the number of samples does not improve the accuracy of the derived statistical quantities (Taylor 1997), because the effective number of independent samples stays constant. Instead, it is advantageous to limit the sampling frequency to $1/(2T_{\text{int}})$ and increase the recording time T.

2.3. Instantaneous quantities

2.3.1. Uncertainty of vorticity. Let us consider a planar-PIV measurement where the velocity components (u, v) are measured in a 2D domain. The out-of-plane vorticity component is defined as:

$$\omega_z = \frac{\partial v}{\partial x} - \frac{\partial u}{\partial y} \quad (39)$$

For sake of brevity, we will drop the subscript z in the reminder and we will indicate the out-of-pane vorticity component simply with ω. The velocity components u and v are discrete functions, defined at grid points with uniform spacing d (both in x- and y-direction). As an example, the vorticity can be computed by the central-difference scheme by:

$$\omega(x,y) = \frac{1}{2d}\left[v(x+d,y) - v(x-d,y) - u(x,y+d) + u(x,y-d)\right] \quad (40)$$

Other methods using larger kernel sizes are available at the expense of lower spatial resolution of the vorticity field. Using the error propagation formula (6), the uncertainty of the vorticity at grid point (x, y) is (apart from truncation errors):

$$U_\omega^2 = \left(\frac{1}{2d}\right)^2 \left[U_v^2 + U_v^2 + U_u^2 + U_u^2 - 2\rho(2d)U_v^2 - 2\rho(2d)U_u^2\right] = 2\left(\frac{1}{2d}\right)^2 \left[1-\rho(2d)\right](U_u^2 + U_v^2) \quad (41)$$

where the following assumptions have been made:

i. The errors of u and v at the same or neighboring spatial locations are uncorrelated (2C-PIV).

ii. The errors of $u(x,\ y+d)$ and $u(x,\ y-d)$ are spatially correlated (and similarly the errors of $v(x+d,\ y)$ and $v(x-d,\ y)$). The corresponding cross-correlation coefficient, indicated with $\rho(2d)$, is assumed to be the same for the two velocity components. It represents the normalized cross-correlation of the measurement error at two grid points at spatial separation $2d$.

iii. The uncertainty of $u(x,\ y+d)$ is assumed to be equal to the uncertainty of $u(x,\ y-d)$ and is indicated with U_u. Likewise, the uncertainty of $v(x+d,\ y)$ is assumed to be equal to the uncertainty of $v(x-d,\ y)$ and is indicated with U_v. In practice, an appropriate local average of uncertainties can be taken.

If we further assume that the two velocity components have the same uncertainty ($U_u = U_v = U$), the expression of the uncertainty of the vorticity simplifies to:

$$U_\omega = \frac{U}{d}\sqrt{1-\rho(2d)} \quad (42)$$

Equation (42) shows the proportionality between the uncertainties of vorticity and velocity. The grid spacing d has a twofold effect on U_ω: on the one hand, U_ω is inversely proportional to d, which would cause a reduction of U_ω when d is increased. On the other hand, increasing d yields a reduction of the spatial cross-correlation coefficient and in turn an increase of the square-root term. When the interrogation window overlap is increased, d tends to zero faster than $\sqrt{1-\rho(2d)}$: as a consequence, the uncertainty of the vorticity increases (see figure 1). However, two things should be kept in mind: (a) equation (42) accounts only for the random errors of the vorticity and not for the truncation errors, which are systematic and decrease when increasing the interrogation window overlap; (b) the uncertainty of the vorticity can be reduced by computing the spatial derivatives using a larger spacing in the finite differences (e.g. using $[v(x+2d,y) - v(x-2d,y)]/4d$ instead of $[v(x+d,y) - v(x-d,y)]/2d$). For noisy data, Vollmers (2001) reports that lower uncertainty can be achieved by computing the vorticity from the flow circulation, rather than via equations (39) and (40). Linear error propagation can be used to evaluate the uncertainty of the vorticity calculated with advanced algorithms; the determination and analysis of that uncertainty goes beyond the scope of the present paper.

It can be shown that equation (42) also corresponds to the uncertainty of the 2D divergence of the velocity. Conversely, for 3D divergence in tomographic PIV, the following expression of the uncertainty is derived:

$$U_{\text{div}} = \frac{U}{d}\sqrt{\frac{3}{2}\left[1-\rho(2d)\right]} \quad (43)$$

The above derivations can be modified accordingly when the central-difference scheme is replaced by more elaborate functions, e.g. fitting flow derivatives by a Levenberg–Marquardt algorithm on a 3×3 or 5×5 vector kernel size. For stereo-PIV with non-zero correlations between u and v, additional terms must be taken into account in the above equations.

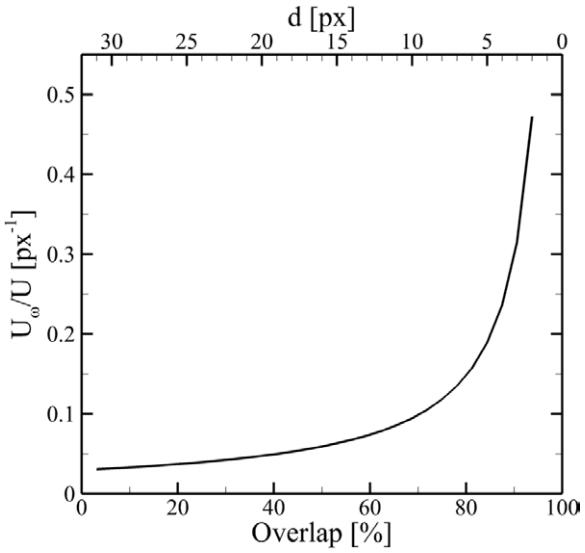

Figure 1. Uncertainty of the vorticity as a function of the interrogation window overlap. Results for interrogation window of size 32 × 32 px^2.

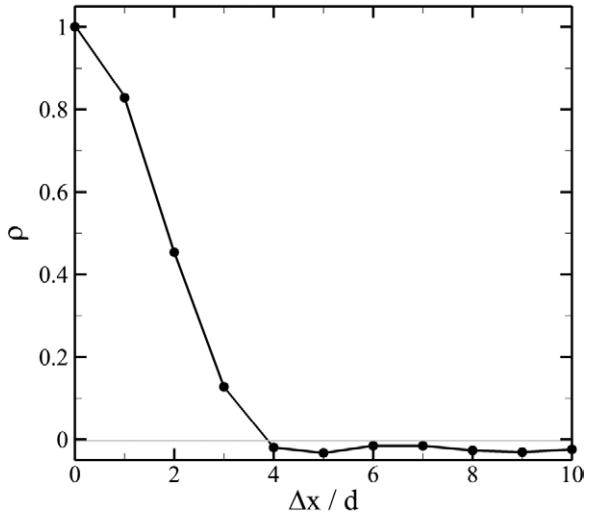

Figure 2. Spatial auto-correlation of the measurement error for interrogation window of 32 × 32 pixels and 75% overlap.

Stereo-PIV uncertainty quantification including assessment of calibration errors will be subject of future work.

2.3.2. Spatially averaged quantities. When a velocity component is spatially averaged over a profile, region or volume, the uncertainty of the average could be computed either by equation (11) using the fluctuations of the velocity vectors, or, alternatively, by considering the mean as a simple function and propagating the individual velocity uncertainties according to equation (6). Usually the second option is preferred, since the mean should be considered here as an instantaneous quantity and not as a statistically converged value. Most often, the underlying mean and standard deviation will be anyway different at different spatial locations. Only in the case of averaging over isotropic homogeneous turbulence with sufficient data points one could try to measure turbulent statistical values; even in this case, it would be more accurate to record a large number of images over time for unbiased statistics.

The derivation of the uncertainty of the mean is done in the same way as in equations (31)–(36), replacing standard deviations with uncertainties, and replacing temporal correlation of velocity components with the spatial correlation of the velocity errors, which are closely related to the spatial resolution of the PIV processing scheme.

Consider the 1D-case with N values of the u velocity component averaged along a profile in x-direction:

$$\overline{u} = \frac{1}{N}\sum_{i=1}^{N} u_i \tag{44}$$

According to equation (6), the uncertainty of the mean is:

$$U_{\overline{u}}^2 = \sum_{i=1}^{N}\sum_{j=1}^{N}\frac{1}{N^2}\rho(\delta u_i, \delta u_j)U_{u_i}U_{u_j} \approx \sum_{i=1}^{N}\sum_{j=1}^{N}\frac{1}{N^2}\rho(\delta u_i, \delta u_j)\overline{U_u^2} \tag{45}$$

where, for simplification, the product of individual uncertainties $U_{u_i}U_{u_j}$ is substituted by the mean square uncertainty $\overline{U_u^2}$. The spatial auto-correlation coefficients $\rho(\delta u_i, \delta u_j)$ can be written as a function of the vector grid spacing d:

$$\rho(\delta u_i, \delta u_j) = \rho\left(|j-i|d\right) = \rho(nd) \tag{46}$$

where n is the number of grid points between locations i and j. Neglecting edge effects, i.e. requiring large N, equation (45) leads to:

$$\begin{aligned} U_{\overline{u}}^2 &= \frac{\overline{U_u^2}}{N^2}\sum_{i=1}^{N}\sum_{n=-\infty}^{+\infty}\rho(nd) = \frac{\overline{U_u^2}}{N^2}N\sum_{n=-\infty}^{+\infty}\rho(nd) \\ &= \frac{\overline{U_u^2}}{N}\sum_{n=-\infty}^{+\infty}\rho(nd) \end{aligned} \tag{47}$$

Again, an effective number of independent samples can be defined as:

$$N_{\mathrm{eff}} = \frac{N}{\sum_{n=-\infty}^{+\infty}\rho(nd)} \tag{48}$$

thus:

$$U_{\overline{u}} = \frac{U_u^{\mathrm{rms}}}{\sqrt{N_{\mathrm{eff}}}} \tag{49}$$

having defined the root-mean-square averaged uncertainty $U_u^{\mathrm{rms}} = \sqrt{\overline{U_u^2}}$.

The integral of the auto-correlation coefficients can be defined as the spatial resolution L_{sr} of the PIV algorithm, which in pixel units is:

$$L_{\mathrm{sr}} = \int_{-\infty}^{+\infty}\rho(x)\mathrm{d}x \tag{50}$$

The spatial resolution can also be written relative to the vector spacing d:

$$L_{\mathrm{sr}}^* = \frac{\int_{-\infty}^{+\infty}\rho(x)\mathrm{d}x}{d} \approx \sum_{n=-\infty}^{+\infty}\rho(nd) \tag{51}$$

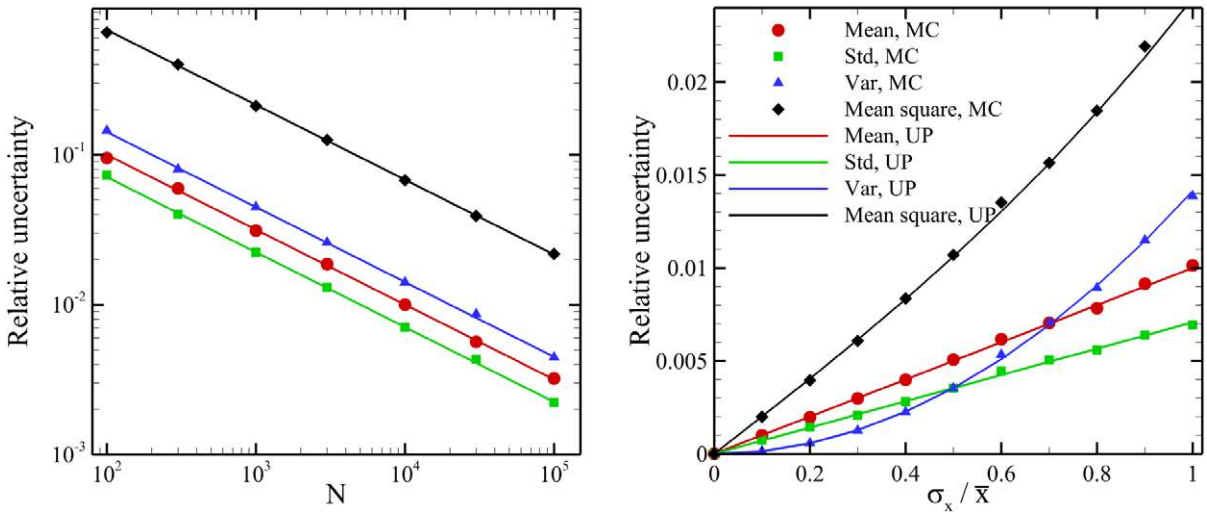

Figure 3. Comparison between the results of Monte Carlo simulations (MC) and uncertainty propagation (UP) for the uncertainty of mean, standard deviation (Std), variance (Var) and mean square. Left: uncertainty as a function of the sample size. Right: uncertainty as a function of the sample standard deviation. For mean and standard deviation, the relative uncertainty is computed dividing the absolute uncertainty by σ_x; for variance and mean square, it is computed dividing the absolute uncertainty by σ_x^2. The symbol keys apply to both plots.

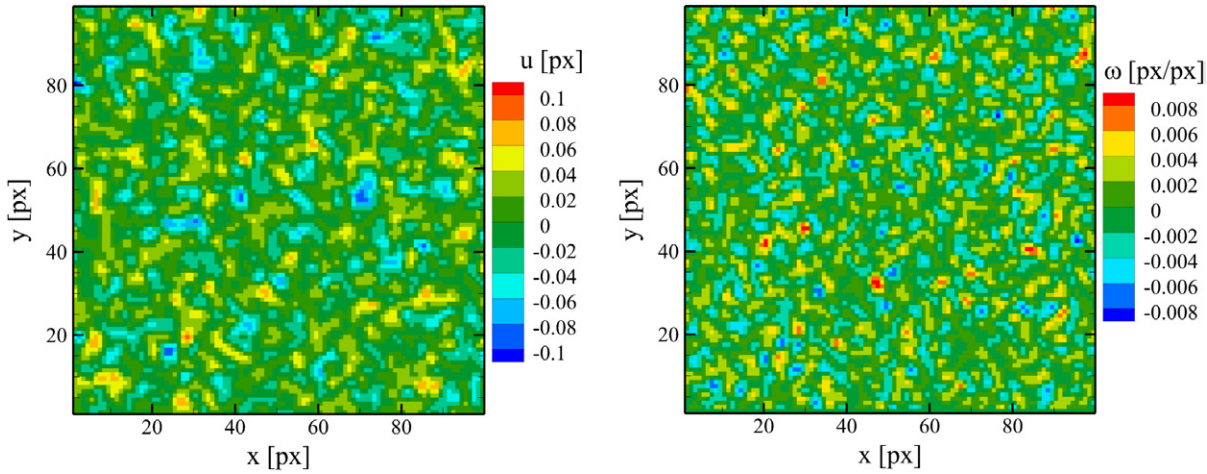

Figure 4. Instantaneous horizontal velocity (left) and vorticity fields (right) for the case $U = 0.1$ px and $\rho = 0.45$.

In the 2D-case, when the average is conducted over a region of $N_x \times N_y$ vectors, equation (48) becomes:

$$N_{\text{eff}} = \frac{N_x N_y}{L_{\text{sr}}^{*\,2}} \tag{52}$$

with L_{sr}^* again in units of vector spacing and assuming the same spatial resolution in x and y. This is, for example, not the case for advanced locally adaptive PIV schemes with elongated windows e.g. adjusting to boundaries. For a single-pass PIV processing scheme with a square interrogation window of $n_{\text{pix}} \times n_{\text{pix}}$ pixel, the correlation function $\rho(x)$ is the triangle function $\left(1 - \frac{|x|}{n_{\text{pix}}}\right)$ for $|x| \leqslant n_{\text{pix}}$, and 0 otherwise. Hence, the spatial resolution is simply $L_{\text{sr}} = n_{\text{pix}}$. For a Gaussian weighted interrogation window with a standard deviation of σ, it can be shown that the spatial resolution is equal to $L_{\text{sr}} = \sqrt{4\pi}\sigma$. For state-of-the-art PIV algorithms using multi-pass window deformation (like DaVis 8), it has been found that the correlation function—when approximating the PIV algorithm as a linear spatial filter function—is Gaussian with some Mexican hat contribution leading to slight overshooting for steep velocity step functions as observed by Elsinga and Westerweel (2011). A detailed analysis is beyond the scope of this work.

In practice, the correlation coefficients and spatial resolution need to be specified for a particular set of PIV processing parameters. When the averaging process is conducted with a small number of vectors over a region comparable to the spatial resolution, the simplifying assumptions that led to equation (49) are not valid anymore. In this case, the uncertainty of the spatial mean must be computed via equation (6), where all individual correlation coefficients must be taken into account.

2.3.3. Spatial correlation of the measurement error. The errors of neighboring vectors are spatially correlated due to the interrogation window overlap. To investigate the spatial correlation of the error, a Monte Carlo simulation is conducted considering

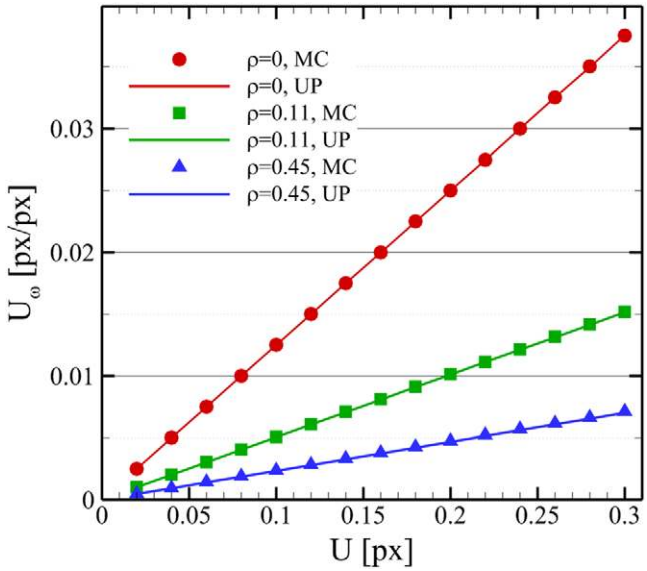

Figure 5. Uncertainty of the vorticity as a function of the uncertainty of the velocity. Comparison between Monte Carlo simulation results (MC) and uncertainty propagation (UP).

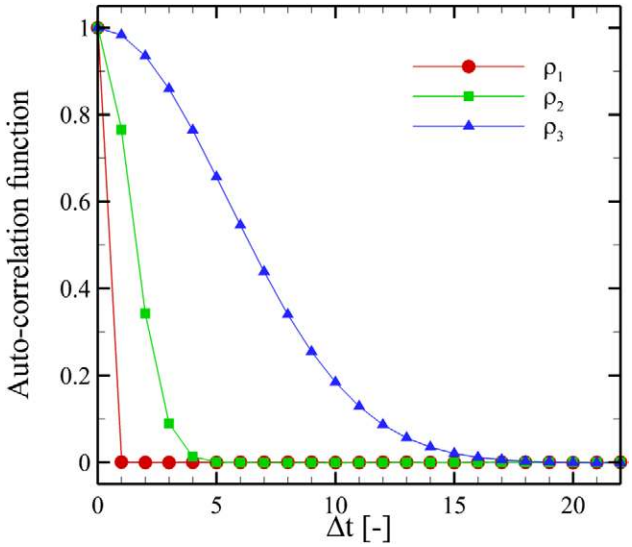

Figure 6. Auto-correlation functions of the three signals. Mean values out of 1000 simulations.

Table 1. Integral time scale and effective number of independent samples for the three signals.

Signal	Total number of samples N	Integral time scale T_{int}	Effective number of samples N_{eff}
x_1	10 000	0.50	10 000
x_2	10 000	1.69	2950
x_3	10 000	6.74	742

a null displacement field. The images have a resolution of 5000 × 400 pixels, with a seeding concentration of 0.05 ppp. The particle images have a Gaussian intensity profile with peak intensity of 1024 counts; their diameter is set to 2 pixels. Noise is added to the recordings (white background noise with 5 counts standard deviation and photon shot noise, assuming a conversion factor of 4 electrons per count) to cause errors in the

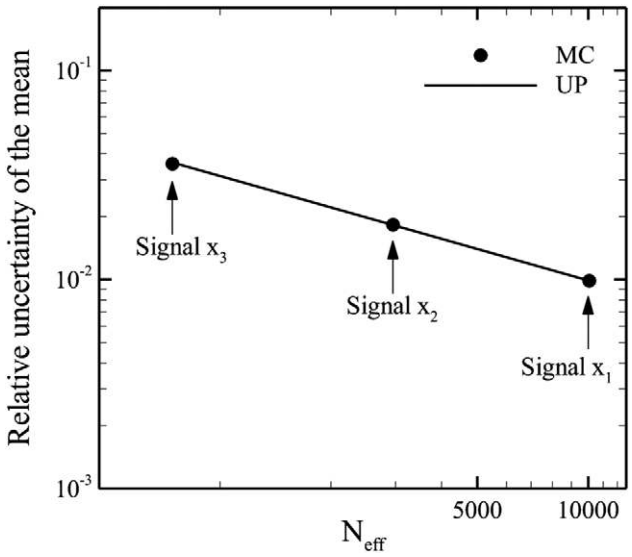

Figure 7. Uncertainty of the mean value (relative to the standard deviation) as a function of the effective number of samples N_{eff}. Comparison between Monte Carlo simulation results (MC) and theoretical uncertainty propagation (UP).

measured velocity. The images are processed with the commercial software DaVis 8.2 from LaVision. The auto-correlation function ρ of the measurement error is computed to investigate the spatial correlation among neighboring vectors. The results of figure 2, which refer to the case of Gaussian-weighted interrogation window size of 32 × 32 pixels with 75% overlap, show that a significant correlation is present up to sample spacing of 3d. Notice that in this case $\rho(2d) \cong 0.45$; hence, the spatial correlation of the error is relevant and cannot be neglected for the computation of the uncertainty of the vorticity via equation (42). Note that the above mentioned mixture of Gaussian and Mexican hat filter function of PIV leads here to the slight undershooting of the correlation values below zero.

3. Numerical assessment via Monte Carlo simulations

3.1. Uncertainty of statistical quantities

The uncertainty of mean, standard deviation, variance and mean square is verified by Monte Carlo simulations. For each sample size N, normally distributed random data are generated with $\overline{x} = 1$ and $\sigma_x = 0.3$, and the statistical quantities of interest are computed. The procedure is repeated 1000 times to evaluate the standard deviation of the mean, standard deviation, variance and mean square. The results of the Monte Carlo simulations are compared with the theoretical predictions of equations (11)–(13) and (22). Figure 3(left) shows the uncertainty as a function of the sample size N: as predicted by the theoretical uncertainty propagation equations, the uncertainty decreases with $1/\sqrt{N}$. The agreement between theoretical values and Monte Carlo simulation is excellent. The simulation is repeated with constant sample size $N = 10\,0000$ and varying the sample standard deviation σ_x (figure 3(right)). The uncertainty of mean, standard deviation and mean square increases linearly with $\sigma_x/\overline{x}$ in the range [0, 1]. Conversely,

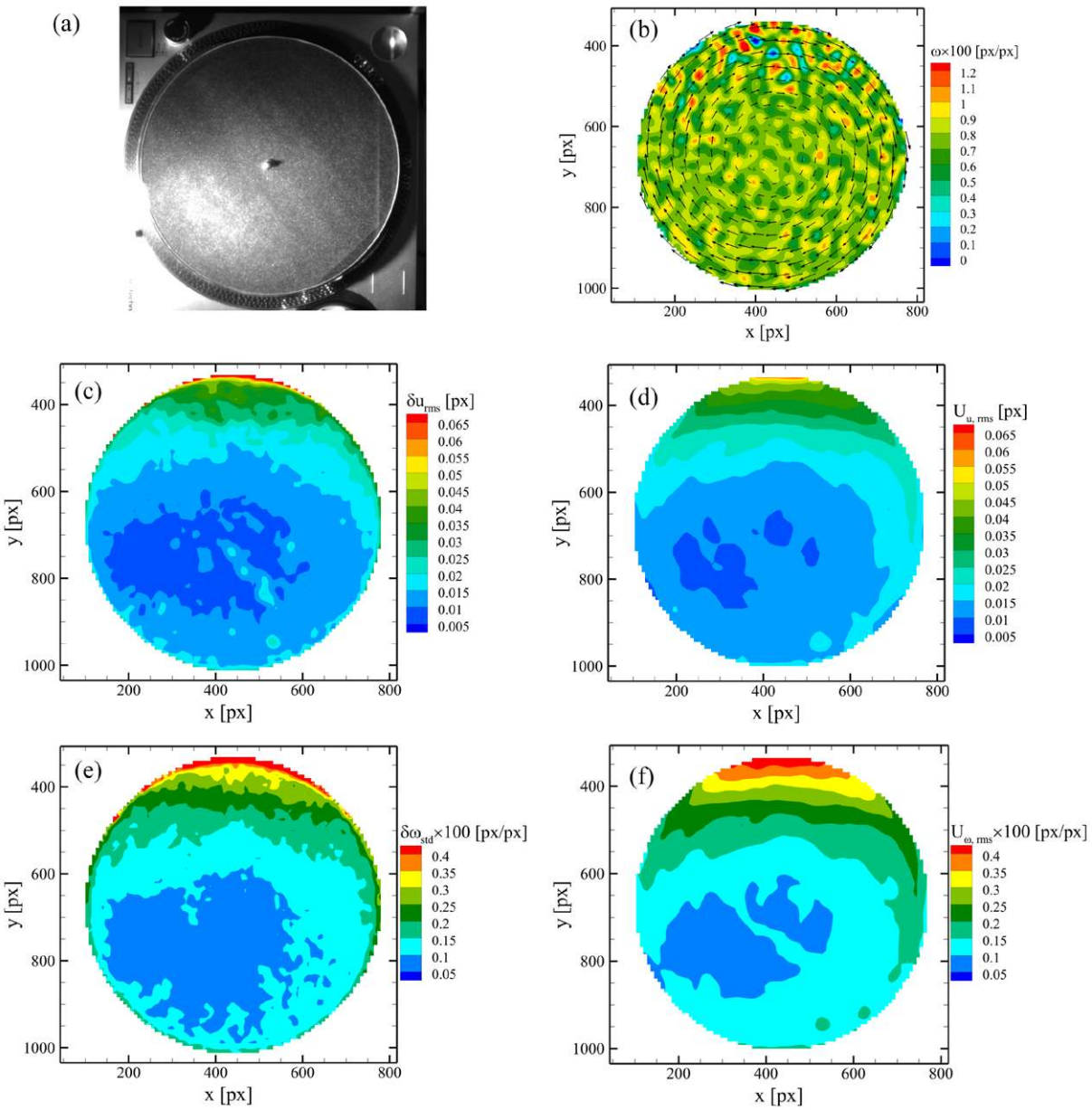

Figure 8. (a) Raw image of the turntable; (b) Measured instantaneous vorticity field with velocity vectors. For sake of clarity, one of 4 vectors is displayed both in x- and y-direction; (c) Root-mean-square of the actual error of the x-displacement; (d) Root-mean-square of the uncertainty of the x-displacement computed with the correlation statistics method; (e) Standard deviation of the actual error of the vorticity; (f) Root-mean-square of the uncertainty of the vorticity, estimated with equation (42).

the uncertainty of the variance features a quadratic increase according to equation (13).

3.2. Uncertainty of vorticity

A Monte Carlo simulation is conducted to assess the accuracy of the uncertainty estimate given by equation (42). A null velocity field ($u = 0$, $v = 0$) is considered on a 2D domain composed by 1000×100 grid points, yielding a null exact vorticity field $\omega = 0$; thus any measured vorticity directly provides the true error. The grid spacing is set to $d = 8$ px, which is the typical value obtained with 32×32 px interrogation windows with 75% overlap. Gaussian noise is added to the velocity field to simulate the error encountered in PIV measurements. The noise is spatially correlated to simulate the effect of interrogation window overlap in PIV. The standard deviation of the noise, which coincides with the measurement uncertainty U, is varied between 0.02 px and 0.3 px. Three values of the cross-correlation coefficient $\rho(2d)$ are considered, namely 0, 0.11, 0.45. These values are representative of the cross-correlation coefficient encountered in PIV for overlap factors of 0%, 50% and 75%. The results are averaged (via root-mean-square) in the entire measurement domain and for a total number of 1000 velocity fields for each value of ρ. An example of instantaneous horizontal velocity field and vorticity field is shown in figure 4.

The results of figure 5 show the excellent agreement between the uncertainty obtained with Monte Carlo simulations and with the theoretical uncertainty propagation (equation (42)). As predicted, the uncertainty of the vorticity

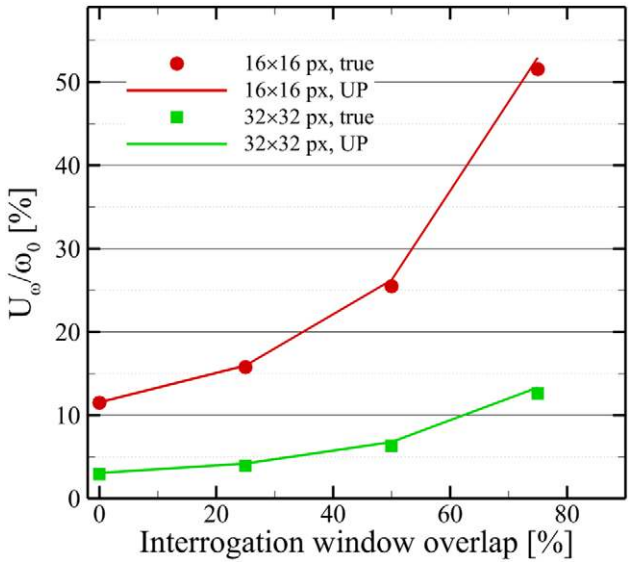

Figure 9. Comparison between true vorticity error and uncertainty propagation (UP) result. Root-mean-square in time over 200 velocity fields and space in the rectangular region $x \in [291; 594]$ px, $y \in [732; 941]$ px.

increases linearly with the uncertainty of the velocity. It is also noticed that the spatial correlation of the measurement error ($\rho = 0.45$) yields a reduction by factor 5 of U_ω with respect to the case where the error is uncorrelated ($\rho = 0$).

3.3. Effective number of independent samples

The influence of the effective number of independent samples on the accuracy of the statistical results in investigated by Monte Carlo simulations. Three signals are considered, each composed by $N = 10\,000$ samples and having actual mean and standard deviation equal to 1.0 and 0.3, respectively. Signal x_1 is composed by statistically independent samples, whereas the samples of signals x_2 and x_3 are statistically dependent. The integral time scale of the signals is evaluated from the auto-correlation function (ρ_1, ρ_2 and ρ_3, respectively) via equation (37) (see figure 6). The effective number of independent samples is then computed via equation (38) and reported in table 1. For each signal, the mean value is computed. The simulation is repeated 1000 times to compute the standard deviation of the estimated mean. The latter is compared with the theoretical prediction of equation (15). The results of figure 7 show the excellent agreement between Monte Carlo simulation and theoretical prediction: the uncertainty of the mean decreases with $1/\sqrt{N_{\text{eff}}}$, even if the total number of samples N is the same for the three signals.

4. Experimental assessment

4.1. Turntable experiment

The first experimental validation has been conducted using a turntable with a diameter of 30 cm rotating at constant speed. A printed pattern with small particles (size of about 200 μm) is applied onto the turn table to simulate flow tracer particles.

Table 2. Parameters of the rectangular jet experiment.

Seeding	Glycol-water droplets, 1 μm diameter
Illumination	Photonics Industries DM40-527 laser
Recording device	MS: LaVision HighSpeedStar 5 CMOS camera
	HDR: 2 × LaVision HighSpeedStar 6 CMOS camera
Imaging	MS: Nikon objective, $f = 105$ mm, $f\# = 4$
	HDR: Nikon objectives, $f = 105$ mm, $f\# = 5.6$
Field of view	MS: 69.3 × 69.3 mm^2
	HDR: 22.8 × 22.8 mm^2
Acquisition frequency	10 000 Hz
Magnification factor	MS: 0.126; HDR: 0.449
Number of images	8000

Images were acquired with a PCO Dimax S4 camera (CMOS sensor, 2016 × 2016 pixel resolution, 11 μm pixel pitch, 12 bit, maximum 1279 frames per second at full resolution), see figure 8(a). The camera mounted a Nikkor lens with 28 mm focal length and the f-number was set to 4.0. The camera was placed at about 1 m distance from the turntable, resulting in a magnification factor of 0.027. A diffusor was mounted between camera and lens to blur the image in order to suppress peak locking errors. The acquisition frequency is 1 kHz with an area of interest of 980 × 1080 pixels. The illumination was provided by an LED light source. The rotational speed of the turntable was set to 37 rpm (0.61 Hz), yielding a uniform vorticity $\omega_0 = 0.007\,58$ px/px. Since the exact vorticity is known, the difference between measured and exact value yields the error of the vorticity. The latter quantity is compared with the uncertainty estimated by the linear propagation (equation (42)).

The images were processed with the LaVision DaVis 8.2 software, using 32 × 32 pixels interrogation window and 75% overlap factor. An instantaneous vorticity field with the velocity vectors is shown in figure 8(b). The root-mean-square of the error of the x-displacement and the standard deviation of the error of the vorticity are shown in figures 8(c) and (e), respectively: both errors are lower in the bottom part of the field of view and increase in the top part due to a reduction of the illumination intensity. The uncertainty of the measured displacement was quantified via the correlation statistics approach (Wieneke 2015). It is verified that the uncertainty U_v of the vertical displacement component (not shown here) is comparable with U_u. The uncertainty of the vorticity is retrieved from the displacement uncertainty via equation (42), using $U = (U_u + U_v)/2$ and $\rho(2d) = 0.45$. Figures 8(d) and (f) show the root-mean-square of the uncertainty of displacement and vorticity, respectively: both results agree very well with the statistical true error (figures 8(c) and (e)) and reproduce the increase of uncertainty from bottom to top of the field of view.

The measurements were repeated for different overlap factors (0%, 25%, 50% and 75%) and interrogation window sizes of 16 × 16 and 32 × 32 px. The uncertainty of the vorticity computed via equation (42) was averaged in space

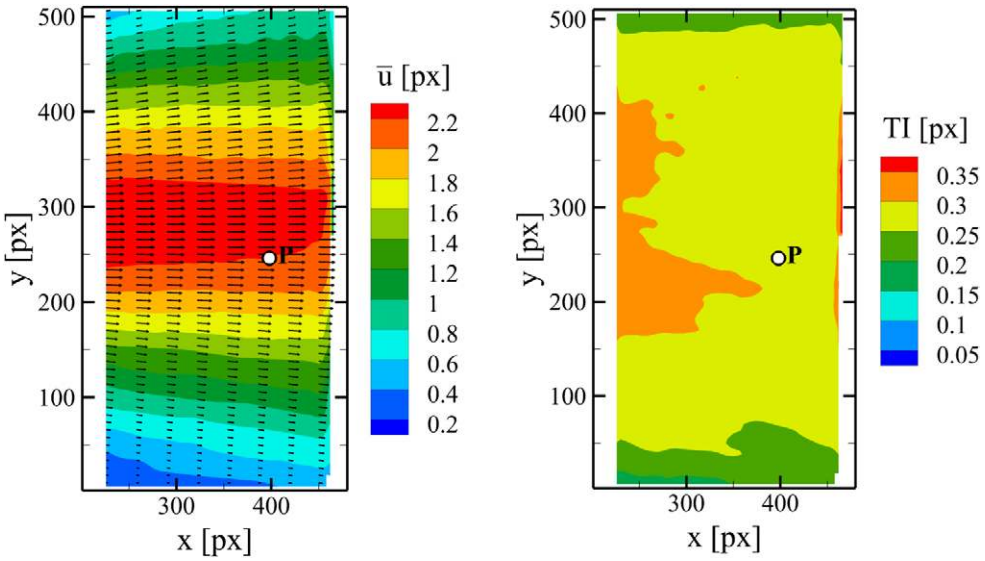

Figure 10. Left: time-average velocity field. For sake of clarity, one every eight vectors is shown in the horizontal direction, one every two in the vertical direction. Right: turbulence intensity.

Table 3. Parameters of the cavity flow experiment.

Seeding	Glycol-water droplets, 1 μm diameter
Illumination	Quantel Evergreen Nd:YAG Laser (200 mJ @ 15 Hz)
Recording device	LaVision Imager LX 2MPx
Imaging	$f = 75$ mm, $f\# = 3.9$
Field of view	$70 \times 55\,\text{mm}^2$
Acquisition frequency	8.33 Hz
Magnification factor	0.093
Number of images	2000

and time over the entire set of 200 fields and compared with the root-mean-square of the vorticity error. The results of the comparison are illustrated in figure 9. The agreement between uncertainty propagation from equation (42) and true uncertainty (stemming from the actual error of the vorticity) is very good. Figure 9 shows that the uncertainty of the vorticity increases with reducing the interrogation window size, because less information carriers are contained in a smaller window. Furthermore, the uncertainty increases with the overlap factor, because a smaller grid spacing d results in larger uncertainty of the vorticity according to equation (42). However, it is important to notice that high overlap factors lead to higher spatial resolution of the vorticity field (smaller d), thus in general to less truncation errors and higher peak vorticity levels at the expense of higher noise.

4.2. Turbulent flow

The uncertainty propagation methodology is applied to two PIV measurements of a turbulent flow. The first one is the rectangular jet flow described in Neal *et al* (2015). The peculiarity of the database is that two PIV measurement systems were used, namely the measurement system (MS) and the high-dynamic range system (HDR). The latter is composed by two cameras in stereoscopic configuration and features a magnification factor larger by factor 3. Via comparison with hot-wire measurements, Neal *et al* (2015) showed that the HDR system yields more accurate results by about factor 4 with respect to the MS. As a consequence, the HDR velocity can be used as a reference to retrieve the error of the MS data. The parameters of the experiment are reported in table 2. The measurements were conducted at $x/h = 20$, being x the streamwise direction and h the jet height, where the turbulent flow is in the turbulent regime.

The MS images were processed with LaVision DaVis 8.2 with 16×16 pixels interrogation window with Gaussian window weighting and 75% overlap factor. For the HDR images, 48×48 pixels interrogation windows with Gaussian weighting and 75% overlap factor were selected. Notice that, due to the difference in optical magnification factor, the different interrogation windows yielded approximately the same spatial resolution for the two systems. The HDR velocity fields were finally mapped onto the MS coordinate system. The time-average velocity field and the turbulence intensity, defined as $\text{TI} = \sqrt{(\sigma_u^2 + \sigma_v^2)/2}$, are shown in figure 10: the turbulence intensity is about 12% of the time-average velocity.

The second experiment is a PIV measurement over a cavity flow. The experiment is conducted in the M-tunnel, a low-speed open-jet open-return wind tunnel of the Aerodynamics Laboratories of TU Delft. The wind tunnel has a squared test section of $40 \times 40\,\text{cm}^2$. The cavity model is made out of wood and has height $H = 2$ cm and spanwise dimension $W = 40$ cm. The length of the cavity is $L = 24$ cm. The free-stream velocity is set to 5 m s^{-1}, yielding a Reynolds number $\text{Re}_H = 6500$ based on the cavity height. A series of 2000 uncorrelated image pairs are acquired at acquisition frequency $f_{\text{acq}} = 8.3$ Hz. The field of view, which is $70 \times 55\,\text{mm}^2$, is positioned 3 H downstream of the beginning of the cavity. The resulting magnification factor is 0.093. The parameters of the cavity flow experiment are reported in table 3. A sketch of the cavity flow

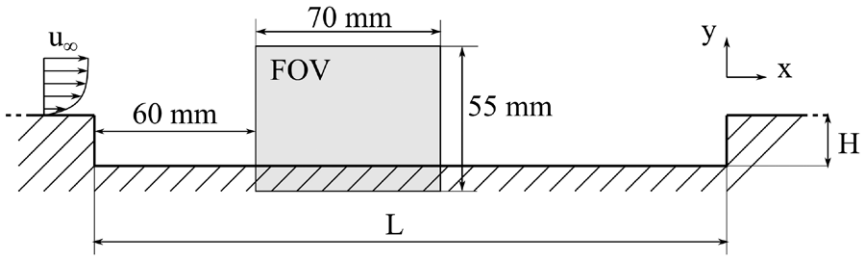

Figure 11. Sketch of the cavity flow experiment.

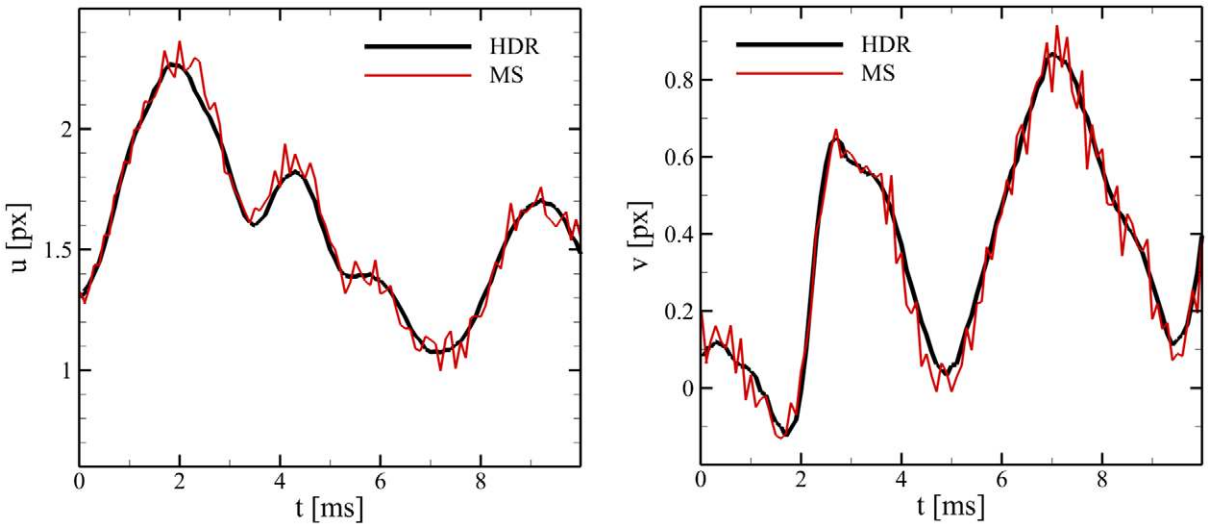

Figure 12. Longitudinal (left) and transverse (right) velocity time series at point P.

Table 4. Actual error and estimated uncertainty at P.

	Mean error	Error standard deviation	Error root-mean-square (rms)	Uncertainty rms
u-component (px)	–0.005	0.060	0.060	0.063
v-component (px)	–0.021	0.060	0.063	0.064
Vorticity (px/px)	0.0008	0.0104	0.0104	0.0116

experiment is shown in figure 11. Further details of the experiment are reported in Iannetta *et al* (2016).

4.2.1. Uncertainty of the vorticity. To assess the uncertainty of the vorticity, the rectangular jet data are used. The velocity time series is extracted at a point P = (398, 246) as shown in figure 10. Figure 12 shows a portion of the time series for a time interval of 10 ms. The comparison between MS and HDR data on the entire time series yields the error for the MS reported in table 4. It is noticed that: (a) the two error components δu and δv have comparable magnitude; (b) the random component of the error (error standard deviation) is significantly larger than the mean bias component.

The vorticity is computed with the central-difference scheme of equation (40), with grid spacing $d = 4$ px. The vorticity time series for the first 10 ms is shown in figure 13. Both

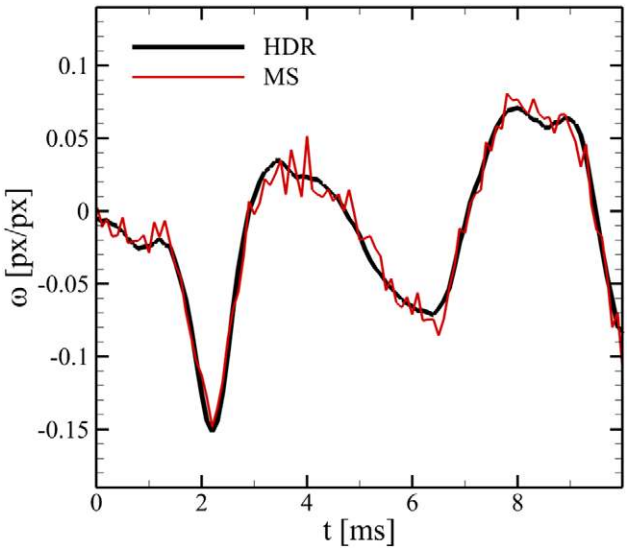

Figure 13. Comparison between MS and HDR vorticity time series at P.

HDR and MS yield the same peak vorticity ($\omega_{max} = -0.15$ px/px at $t = 2.2$ ms), which confirms that the two systems have the same spatial resolution. The vorticity error $\delta\omega$ is computed as the difference between MS and HDR vorticity. The results of table 4 show that the random error dominates over the mean bias error.

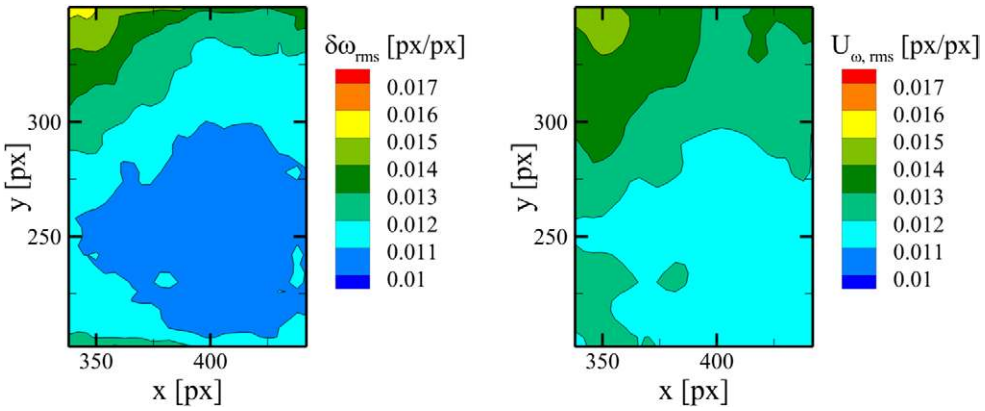

Figure 14. Comparison between root-mean-square of the vorticity error (left) and root-mean-square of the estimated vorticity uncertainty (right).

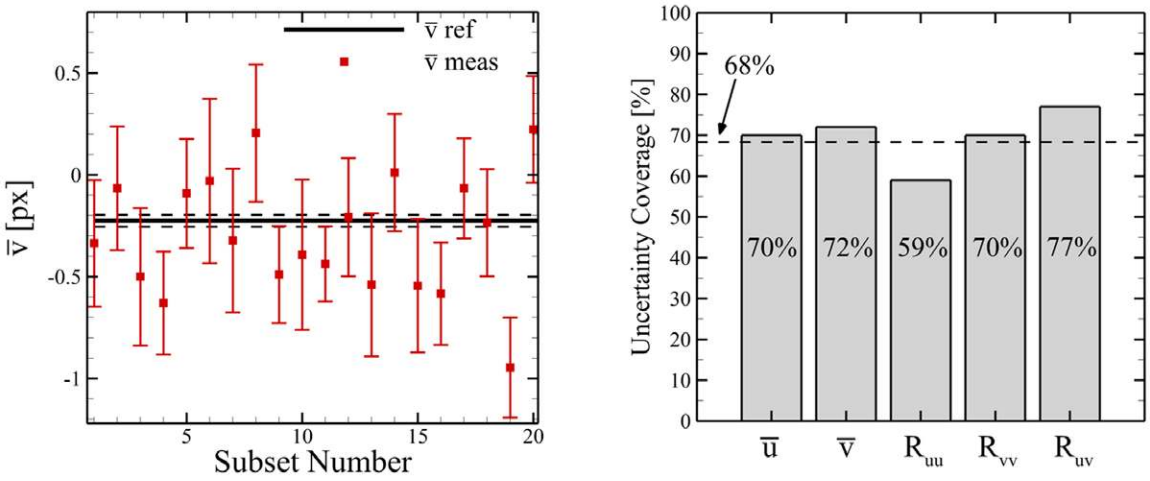

Figure 15. Left: comparison between time-averaged vertical velocity obtained with the subsets of 20 samples and that computed with the entire set of 2000 samples. For sake of clarity, only the first 20 subsets (out of 100) are shown. The uncertainty bars are evaluated at 68% confidence level with the corresponding uncertainty propagation formula. The uncertainty of the reference value is displayed with a dashed black line. Right: uncertainty coverage for different statistical quantities. The theoretical uncertainty coverage for Gaussian error distribution is 68%.

The uncertainty at P is evaluated with the correlation statistics method (Wieneke 2015). Uncertainty propagation is done according to equation (42) using $d = 4$ px, $U = (U_u + U_v)/2$ and $\rho(2d) = 0.45$. The root-mean-square of the uncertainty is equal to $U_{u,\mathrm{rms}} = 0.063$ px and $U_{v,\mathrm{rms}} = 0.064$ px, which agrees very well with the error root-mean-square of 0.060 and 0.063, respectively. The calculation is repeated in the entire measurement domain in common between HDR and MS. The contours of figure 14 illustrate the comparison between the rms of the error and the uncertainty of the vorticity. Both uncertainty and error exhibit small variations within the considered domain, with values between 0.010 and 0.016 px/px. Again, the agreement between estimated uncertainty and error is very good.

4.2.2. Uncertainty of statistical quantities. The time-resolved jet data are not suited for statistical analysis because the low effective number of independent samples ($N_{\mathrm{eff}} = 243$, despite the total number of samples is $N = 8000$) does not guarantee the statistical convergence of the results. Hence, to assess the uncertainty of statistical flow properties, the cavity flow data are used, where 2000 statistically independent velocity field are available.

Velocity data are extracted at a point P located close to the reattachment point; the turbulence intensity in P is equal to 22.0% of the free-stream velocity. The entire set of 2000 samples is divided into 100 independent subsets composed by 20 samples each. The statistical flow properties, namely time averages and Reynolds stresses, are computed from the subsets and compared with the value obtained with the entire set. Figure 15(left) shows the comparison between the time-averaged vertical velocity computed with the subsets of 20 samples and that evaluated from the entire set of 2000 samples. The uncertainty bars are evaluated with equation (15) and correspond to a theoretical confidence level of 68%. In most of the cases the results agree within the uncertainty of the measured mean velocity. To assess the accuracy of the uncertainty propagation formulae, the uncertainty coverage for different statistical quantities is computed and displayed in figure 15(right). The uncertainty

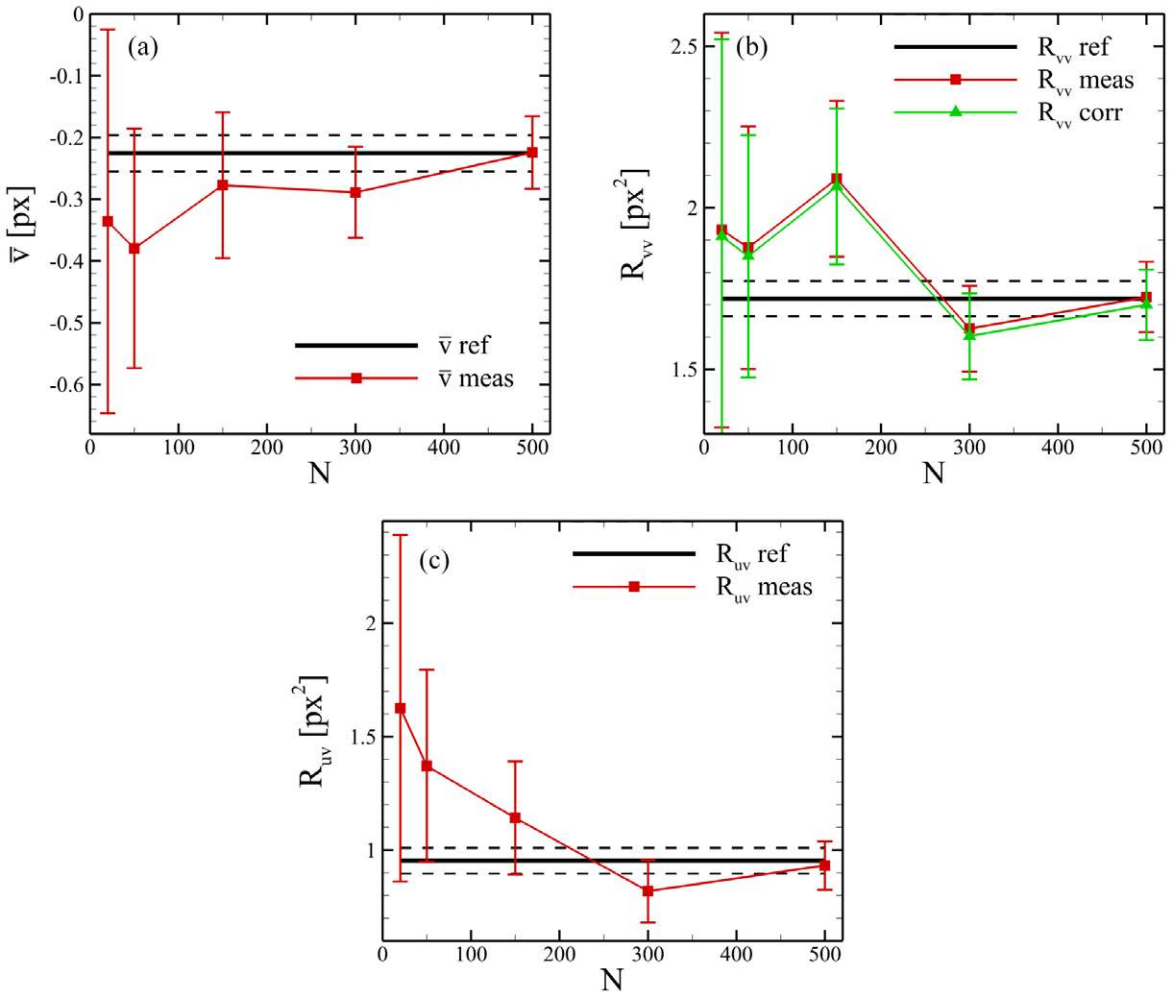

Figure 16. (a) Convergence of the mean vertical velocity as a function of the sample size. (b) Convergence of the Reynolds normal stress as a function of the sample size. (c) Convergence of the Reynolds shear stress as a function of the sample size. In all plots, the uncertainty bars are evaluated at 68% confidence level with the corresponding uncertainty propagation formula. The uncertainty of the reference value is displayed with a dashed black line.

coverage is defined as the number of samples for which the error is smaller than or equal to the estimated uncertainty. In case of Gaussian error distribution, the theoretical uncertainty coverage is about 68%. The results of figure 15(right) show the accuracy of the uncertainty propagation methodology: the uncertainty of the time-averaged quantities ($\overline{u}$ and $\overline{v}$) is accurate within 5%, whereas that of the Reynolds stresses is accurate within 10%.

The effect of the number of samples on the accuracy of the statistical results is shown in figure 16. It is evident that the random uncertainty of the mean (figure 16(a)) is initially large and decreases with increasing sample size. In the entire range of sample sizes considered, the reference mean velocity is within the uncertainty bounds estimated with equation (15). Similarly, the normal Reynolds stress R_{vv} converges to the reference value with rate $1/\sqrt{N}$ (figure 16(b)). For low sample size ($N < 250$), the measured R_{vv} overestimates the reference value due to the effect of spurious fluctuations by about 10%. A corrected value of R_{vv} is computed by subtracting the mean-square fluctuation: $R_{vv,\mathrm{corr}} = R_{vv} - U^2_{\mathrm{rms}}$. The uncertainty of uncorrected and corrected R_{vv} is computed via equations (18) and (23), respectively. The two uncertainties are the same within 1%, meaning that the uncertainty of R_{vv} is mainly due to statistical convergence rather than to the measurement uncertainty of u and v. For a correction of less than 1%, one would need at least 20 000 independent samples according to equation (24) before the uncertainty of the Reynolds stress decreases to the same level as the correction term U^2_{rms}. But a correction is nevertheless useful for low levels of Reynolds stress comparable to the uncertainties.

The Reynolds shear stress R_{uv} is illustrated in figure 16(c). To compute the uncertainty $U_{R_{uv}}$, the cross-correlation coefficient between u and v is calculated: $\rho_{uv} = 0.41$. The measured R_{uv} converges to the reference value with rate $1/\sqrt{N}$. As the estimated uncertainty, also the measurement error (difference between measured and reference value) decreases with increasing the sample size.

5. Conclusions

The present study proposes a mathematical framework for the propagation of the instantaneous measurement uncertainty to derived quantities of interest, either instantaneous (e.g. velocity derivatives, vorticity, divergence) or statistical (mean, Reynolds stresses, TKE). The framework relies upon the use of linear error propagation.

For statistical quantities, the uncertainty is typically dominated by random errors due to the finite sample size. The uncertainty decreases with $1/\sqrt{N_{\mathrm{eff}}}$, being N_{eff} the effective number of independent samples. It is noticed that, in many PIV experiments conducted in continuous rate mode, N_{eff} may be significantly lower than the total number of samples N, thus yielding an uncertainty of statistical quantities larger than that obtained when the samples are statistically independent. The quantification of the uncertainty of statistical quantities does not require the knowledge of the uncertainty of the instantaneous velocity fields. Nevertheless, the instantaneous uncertainty allows correcting the normal Reynolds stress for the spurious fluctuations due to random errors. In fact, in absence of systematic errors due to peak locking or spatial modulation, the random errors have the effect to increase the measured normal Reynolds stress with respect to the actual one. The uncertainty of velocity spatial derivatives (e.g. vorticity and divergence) depends upon the spatial correlation of the measurement error along x- and y-directions. The latter is related to the measurement spatial resolution, which can be evaluated from the sum of the error spatial auto-correlation values. Although the error correlation is typically unknown in an experiment, it can be estimated *a priori* by Monte Carlo simulations for a given set of PIV processing parameters.

The proposed uncertainty propagation methodology is assessed via both Monte Carlo simulations and experiments. The Monte Carlo simulations showed the accuracy of the estimated uncertainty for varying testing conditions (sample size, signal variance, error correlation) under the assumption of Gaussian error distribution of the velocity. In the experimental assessment, the reference velocity is either known (turntable experiment) or estimated with an auxiliary PIV system featuring a higher dynamic range (turbulent flow experiment), as done in Neal *et al* (2015), or evaluated with a much larger sample size for statistical convergence. From the experimental assessment, three main conclusions can be drawn:

i. When the spatial correlation of the error is correctly taken into account, the uncertainty of the vorticity is estimated typically within 5–10% accuracy.
ii. When the actual flow fluctuations are larger than the instantaneous uncertainties, the uncertainty of statistical quantities is dominated by the finite sample size rather than the random instantaneous uncertainties.
iii. the uncertainty of the time-averaged quantities ($\overline{u}$ and $\overline{v}$) is accurate within 5%, whereas that of the Reynolds stresses is accurate within 10%.

References

Ahn S and Fessler J A 2003 Standard errors of mean. Variance and standard deviation estimators http://web.eecs.umich.edu/~fessler/papers/files/tr/stderr.pdf

Bendat J S and Piersol A G 2010 *Random Data—Analysis and Measurement Procedures* 4th edn (Hoboken, NJ: Wiley)

Benedict L H and Gould R D 1996 Towards better uncertainty estimates for turbulence statistics *Exp. Fluids* **22** 129–36

Charonko J J and Vlachos P P 2013 Estimation of uncertainty bounds for individual particle image velocimetry measurements from cross-correlation peak ratio *Meas. Sci. Technol.* **24** 065301

Coleman H W and Steele W G 2009 *Experimentation, Validation, and Uncertainty Analysis for Engineers* 3rd edn (Hoboken,NJ: Wiley)

Elsinga G E and Westerweel J 2011 The point-spread-function and the spatial resolution of PIV cross-correlation methods *Nineth Int. Symp. on Particle Image Velocimetry (Tsukuba, Japan, 21–23 July)*

George W K, Beuther P D and Lumley J L 1978 Processing of random signals *Proc. of the Dynamic Flow Conf. 1978 on Dynamic Measurements in Unsteady Flows* (Netherlands: Springer)

Iannetta F, Sciacchitano A, Arpino F and Scarano F 2016 Numerical and experimental comparison of velocity derived quantities in rectangular cavity flows *Fourth Int. Conf. on Computational Methods for Thermal Problems THERMACOMP2016 (6–8 July 2016)* (Atlanta: Georgia Tech)

Neal D R, Sciacchitano A, Smith B L and Scarano F 2015 Collaborative framework for PIV uncertainty quantification: the experimental database *Meas. Sci. Technol.* **26** 074003

Sciacchitano A, Neal D R, Smith B L, Warner S O, Vlachos P P, Wieneke B and Scarano F 2015 Collaborative framework for PIV uncertainty quantification: comparative assessment of methods *Meas. Sci. Technol.* **26** 074004

Sciacchitano A, Wieneke B and Scarano F 2013 PIV uncertainty quantification by image matching *Meas. Sci. Technol.* **24** 045302

Taylor J R 1997 *An Introduction to Error Analysis: the Study of Uncertainties in Physical Measurements* (Sausalito, CA: University Science Books)

Tennekes H and Lumley J L 1972 *A First Course in Turbulence* (Cambridge, MA: MIT Press)

Timmins B H, Wilson B W, Smith B L and Vlachos P P 2012 A method for automatic estimation of instantaneous local uncertainty in particle image velocimetry measurements *Exp. Fluids* **53** 1133–47

Vollmers H 2001 Detection of vortices and quantitative evaluation of their main parameters from experimental velocity data *Meas. Sci. Technol.* **12** 1199

Wieneke B 2015 PIV uncertainty quantification from correlation statistics *Meas. Sci. Technol.* **26** 074002

Wilson B M and Smith B L 2013a Taylor-series and Monte-Carlo-method uncertainty estimation of the width of a probability distribution based on varying bias and random error *Meas. Sci. Technol.* **24** 035301

Wilson B M and Smith B L 2013b Uncertainty on PIV mean and fluctuating velocity due to bias and random errors *Meas. Sci. Technol.* **24** 035302

Xue Z, Charonko J J and Vlachos P P 2014 Particle image velocimetry correlation signal-to-noise ratio metrics and measurement uncertainty quantification *Meas. Sci. Technol.* **25** 115301